ARTICLES
PUBLISHED ONLINE: 21 JULY 2013 | DOI: 10.1038/NPHOTON.2013.174
nature photonics

Tenfold reduction of Brownian noise in high-reflectivity optical coatings

Garrett D. Cole[1,2†*], Wei Zhang[3†], Michael J. Martin[3], Jun Ye[3*] and Markus Aspelmeyer[1*]

Thermally induced fluctuations impose a fundamental limit on precision measurement. In optical interferometry, the current bounds of stability and sensitivity are dictated by the excess mechanical damping of the high-reflectivity coatings that comprise the cavity end mirrors. Over the last decade, the dissipation of these amorphous multilayer reflectors has at best been reduced by a factor of two. Here, we demonstrate a new paradigm in optical coating technology based on direct-bonded monocrystalline multilayers, which exhibit both intrinsically low mechanical loss and high optical quality. Employing these 'crystalline coatings' as end mirrors in a Fabry–Pérot cavity, we obtain a finesse of 150,000. More importantly, at room temperature, we observe a thermally limited noise floor consistent with a tenfold reduction in mechanical damping when compared with the best dielectric multilayers. These results pave the way for the next generation of ultra-sensitive interferometers, as well as for new levels of laser stability.

Today's most advanced technologies for measuring time and space[1], particularly optical atomic clocks[2,3] and interferometric gravitational wave detectors[4], are now encountering an ultimate barrier set by fundamental thermal processes. These systems rely on optical interferometry, where thermally driven fluctuations result in modifications of the optical path length and hence unavoidable 'thermal noise'[5]. The need to minimize these effects has led to major advances in the design of optical cavities, which have continually redefined the state of the art in optical precision sensing[6–12]. The most significant remaining impediment for achieving enhanced performance is the Brownian motion of the cavity's high-reflectivity multilayer coatings[10,13,14]. According to the fluctuation–dissipation theorem[15,16], this motion is directly linked to mechanical damping in the constituent materials of the coating. Thus, the long-standing challenge has been to identify materials simultaneously capable of high reflectivity and low mechanical dissipation. However, the mechanical damping of existing dielectric multilayer mirrors has remained unacceptably large, with a maximum reduction in the overall loss of 50% in recent years[17]. Building on advancements in semiconductor lasers[18], quantum optomechanics[19] and microfabrication[20], in this Article we demonstrate low-loss mirrors based on substrate-transferred epitaxial multilayers, which exhibit both unprecedentedly low mechanical loss and high optical quality, enabling an order of magnitude reduction in coating Brownian noise.

Optical precision measurement relies on the accurate sensing of changes in phase of a probe laser beam, which in turn requires ultrastable optical interferometers. The best performance to date is achieved with mirrors implementing high-reflectivity multilayer coatings on transparent substrates, both of which exhibit subnanometre surface roughness. Dielectric SiO_2/Ta_2O_5 multilayers deposited by ion beam sputtering (IBS) have represented the state of the art in high-reflectivity optical coatings since the 1980s, with optical absorption at the parts-per-million (ppm) level[21]. This has led to enormous progress in a broad range of applications including subattometre displacement sensitivities for gravitational wave observatories[4] and frequency stabilities at the 1×10^{-16} level for metrology applications[9–11].

In spite of their superior optical properties, the amorphous thin films at the heart of these coatings exhibit excess mechanical damping[22,23] driven by the internal losses in the high-index tantala (Ta_2O_5) layers[24]. This results in significant displacement fluctuations of the mirror surface arising from thermally driven mechanical modes, typically referred to as 'coating thermal noise'[25]. In general, the magnitude of such Brownian motion can be quantified via the frequency-dependent noise power spectral density (NPSD), $G_x(f)$, and depends strongly on mechanical damping in the material system. Specifically, $G_x(f) \propto k_B T \cdot \phi \cdot 1/f$ (where k_B is the Boltzmann constant, T is temperature and f is Fourier frequency in the low-frequency limit far from any mechanical resonances of the system), where the mechanical loss angle ϕ, given by the imaginary component of a complex Young's modulus $E(f) = E_0[1 + i\phi(f)]$, characterizes the energy dissipation rate. The overall Brownian noise floor is determined by the loss angle contributions of all cavity components, namely the substrate ϕ_{sub}, spacer ϕ_{spacer} and coating ϕ_c (ref. 13). This is the essence of the fluctuation–dissipation theorem in its application to optical interferometry. An independent source of significant coating-related noise arises from thermal fluctuations in the multilayer and substrate driven by the finite thermal expansion coefficient[26], as well as through the temperature dependence of the index of refraction of the constituent films[27], referred to as thermo-elastic and thermo-refractive noise, respectively. In stark contrast to Brownian noise, these 'thermo-optic' noise sources add coherently and can in principle be eliminated by careful design of the layer structure of the mirror[28,29].

The most significant improvements in optical cavity performance have resulted from direct attempts to minimize the thermal noise, chiefly by choosing substrates with minimal damping, as well as by reducing the environmental temperature. Currently, the best room-temperature reference cavity performance[11] is achieved by combining an ultralow-expansion (ULE) glass spacer ($\phi_{ULE} = 1.7 \times 10^{-5}$) (ref. 13) with fused silica substrates

[1]Vienna Center for Quantum Science and Technology (VCQ), Faculty of Physics, University of Vienna, A-1090 Vienna, Austria, [2]Crystalline Mirror Solutions GmbH, A-1090 Vienna, Austria, [3]JILA, National Institute of Standards and Technology and University of Colorado, Boulder, Colorado 80309-0440, USA; [†]These authors contributed equally to this work. *e-mail: garrett.cole@univie.ac.at; ye@jila.colorado.edu; markus.aspelmeyer@univie.ac.at

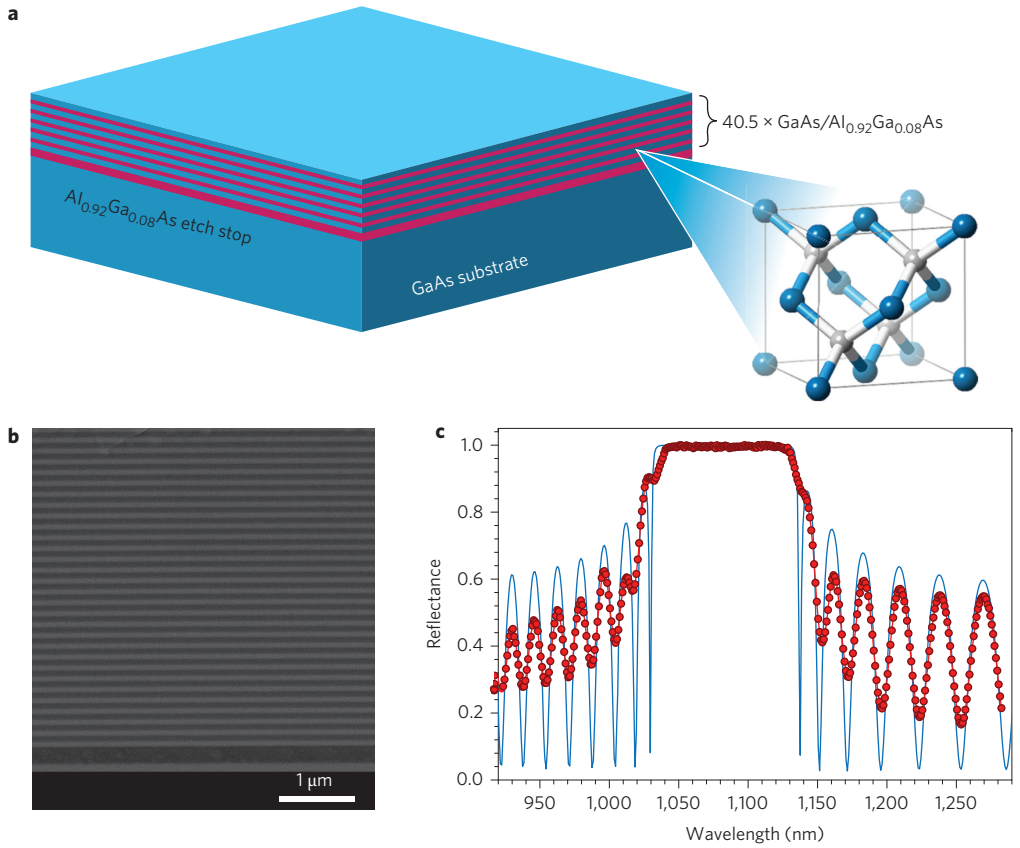

Figure 1 | Design of the room-temperature 1,064 nm AlGaAs Bragg mirror. a, Cross-sectional schematic of the crystalline multilayer. Inset: the zincblende unit cell (space group $T_d^2 - F\bar{4}3m$). The mirror consists of a total of 81 layers (thickness, 6.83 μm) of alternating quarter-wave GaAs (high index, 3.480) and $Al_{0.92}Ga_{0.08}As$ (low index, 2.977) grown on a (100)-oriented GaAs substrate via MBE. The base of the mirror incorporates a 270-nm-thick $Al_{0.92}Ga_{0.08}As$ etch stop layer for protection during the substrate removal process. **b**, Scanning electron micrograph of a cleaved facet of the epitaxial structure, demonstrating smooth and abrupt interfaces. The etch stop can be seen as the dark band above the legend. **c**, Fitted reflectance spectrum (red points, spectrophotometer measurements; blue line, transmission matrix theory) of the AlGaAs multilayer after transfer to a glass carrier. An excellent fit is achieved, with the absolute reflectance value limited by the wavelength resolution (1 nm) of the instrument.

($\phi_{silica} = 1 \times 10^{-6}$) (refs 13, 26) (note that lower losses have been observed in high-quality silica samples[30], but typical mirror blanks are abrasively polished with an unfinished barrel and will thus likely yield the quoted loss angle value). Such a structure is limited primarily by the dielectric multilayer, with $\phi_{dielectric} \approx 4 \times 10^{-4}$ (ref. 13). In cryogenic systems, for example, the recently demonstrated single-crystal silicon cavity (spacer and substrates, $\phi_{Si} = 1 \times 10^{-8}$ at 124 K), the coating Brownian noise becomes the sole limiting factor in the laser frequency stability[10]. In an entirely different operating regime, gravitational wave detectors are limited in their most sensitive measurement band by the coating thermal noise introduced by the lossy dielectric multilayers[25]. It is fascinating to realize that the performance of a 4-km-long interferometer is limited by a ~5-μm-thick surface coating.

Progress in minimizing the excessively large coating loss angle, unfortunately, has been modest. The best reported value to date for IBS-deposited dielectric multilayers is 2×10^{-4} through the incorporation of a small fraction of TiO_2 into the high-index tantala layers[17]. Even with this improvement, the large loss angle will still remain the dominant noise source for reference cavities and gravitational wave detectors. For this reason, interferometer designs have used workarounds that minimize the overall sensitivity to thermal noise. This can be achieved in several ways: by lengthening the cavity[11,31], as fractional fluctuations in the centre frequency scale inversely with the total optical path length; by increasing the size of the optical mode[31,32], as sampling a larger area of the mirror surface effectively averages out small-scale fluctuations; or by exploiting the coherent character of the underlying displacements and strains for potential cancellation[33]. Unfortunately, these workarounds either significantly complicate the system design or lead to excessively large cavities with increased vibration sensitivity. In a similar vein, various proposals have been put forward to significantly alter or even eliminate the coating entirely; these include resonant waveguide grating reflectors[34], photonic-crystal reflectors[35], ring cavities and whispering-gallery-mode (WGM) resonators[36]. These approaches, however, have not yet demonstrated both a sufficiently high mechanical quality and sufficiently narrow cavity linewidth. Ultimately, the next generation of advanced interferometric systems will only be possible through solutions that address the mechanical properties of the coating itself.

Recent work in quantum optomechanics has provided a completely different route to a solution. This field of research exploits optomechanical interactions within optical cavities to control and study the quantum regime of nano- to macroscale mechanical oscillators[19]. Similar to the requirements discussed here, reaching the quantum regime of mechanical motion necessitates the implementation of structures with both high optical and mechanical quality. In this context, monocrystalline $Al_xGa_{1-x}As$ heterostructures (AlGaAs) have been identified as a promising option for multilayer mirrors, in particular, because this materials system is capable of significantly reduced loss angles[37,38]. AlGaAs-based epitaxial distributed Bragg reflectors (DBRs) have been applied for the fabrication of

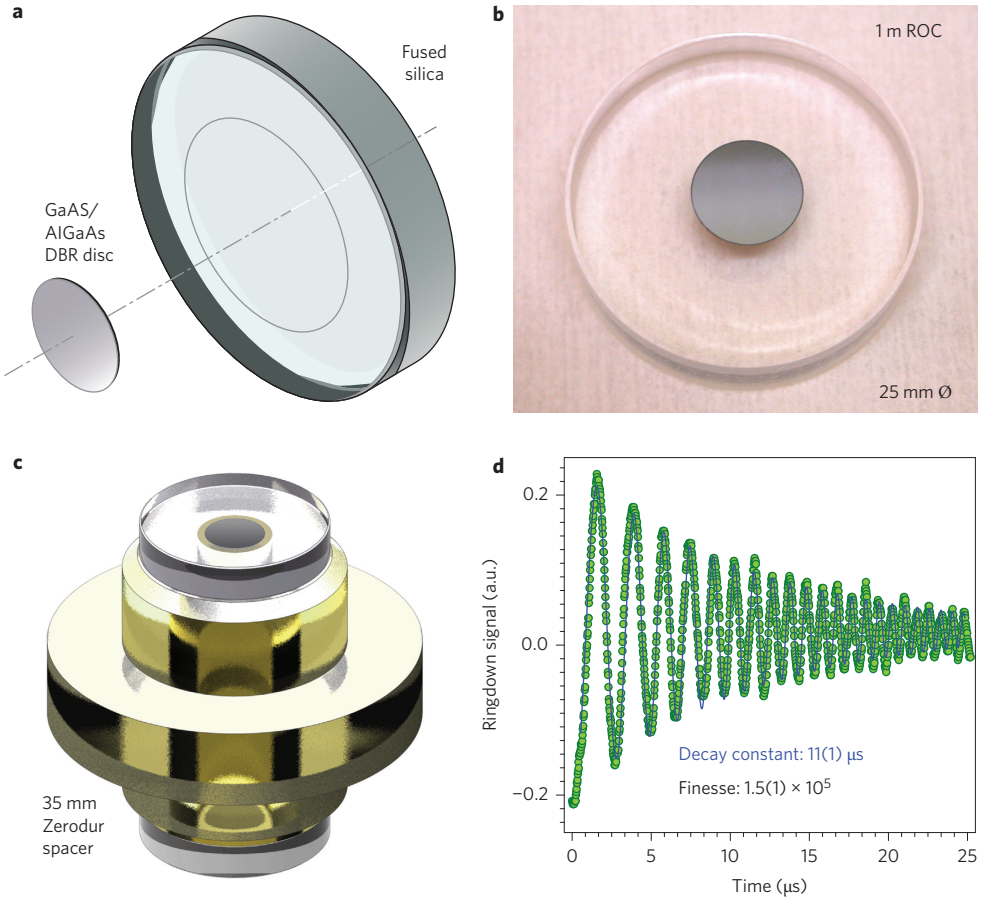

Figure 2 | Construction of an optical reference cavity using substrate-transferred crystalline coatings. a, Exploded view of a bonded mirror assembly, showing the AlGaAs mirror disc and fused-silica substrate with a polish-imparted 1 m ROC. **b**, Photograph of the front face of a completed curved mirror assembly incorporating a bonded 8-mm-diameter epitaxial DBR on a 25-mm-diameter fused-silica substrate with a 1 m ROC. This sample shows a clean and defect-free bond interface with an absence of Newton's rings between the AlGaAs and fused silica. **c**, Solid model of a cavity constructed from two bonded mirror assemblies (one planar and one with a 1 m ROC) optically contacted to a 35-mm-long Zerodur spacer. **d**, Swept laser frequency ringdown of the optical cavity field in reflection, yielding a finesse of 1.5(1) × 10^5 at 1,064 nm (green points, measurements; blue line, theoretical fit) and demonstrating the excellent optical properties of the bonded crystalline coating.

vertical-cavity surface-emitting lasers (VCSELs) since the late 1980s[39], but the mechanical damping has not been studied in detail until recently. Ring-down measurements on free-standing mechanical resonators microfabricated directly from epitaxial AlGaAs multilayers have yielded exceptional quality factors Q of up to 40,000 at room temperature[38]. For an isolated resonance, Q can be converted to loss angle via $\phi_{\mathrm{AlGaAs}} = Q^{-1} \approx 2.5 \times 10^{-5}$. In comparison, measured Q values for free-standing SiO_2/Ta_2O_5 fall in the range of a few thousand[40], yielding values consistent with the coating loss angles observed in studies of such mirrors for optical reference cavities and gravitational wave detectors[22–24]. Taking into account the competitive optical performance of AlGaAs-based DBRs, with reflectivity values routinely surpassing 0.9998 (refs 37, 38), these epitaxial multilayers represent a promising alternative for the development of mirror structures with ultra-low thermal noise.

Although excellent optomechanical properties have been demonstrated in suspended micrometre-scale resonators, it is not immediately clear as to how these epitaxial multilayers can be deployed as high-performance macroscopic mirrors. In particular, lattice matching constraints preclude the deposition of monocrystalline films onto amorphous substrates due to the lack of a crystalline template for seeded growth. An additional difficulty arises as stable optical cavities require curved mirrors, the realization of which is incompatible with the current capabilities of high-quality epitaxial film growth. Such limitations are not found with sputtered dielectric mirrors, which can be deposited on essentially any relevant, and even structured, substrate.

Nonetheless, by exploiting advanced semiconductor microfabrication processes, we have realized a successful implementation of this low-loss materials system in a standard optical reference cavity configuration. To generate the crystalline coatings, we use a direct-bonding process that builds upon foundational work such as semiconductor 'wafer fusion'[41], which has enabled the production of various engineered substrates[42] (for example, bonded silicon-on-insulator), as well as early demonstrations of epitaxial layer transfer[43,44] and more recent stamp-mediated methods[20] aimed at the development of novel micro- and optoelectronic systems. At its most basic level, these processes are analogous to optical contacting, a widely used bonding approach that is routinely applied in the construction of optical subassemblies.

Results

Fabrication and optical characterization. Our fabrication process begins with the growth of a high-quality epitaxial Bragg mirror on a GaAs substrate (Fig. 1). The multilayer used in this experiment (Fig. 1a) is a standard quarter-wave design, with alternating high- and low-index layers generated by modulating the Al content of the constituent films. Using molecular beam epitaxy (MBE), we deposited high-quality epilayers (Fig. 1b) exhibiting a low-

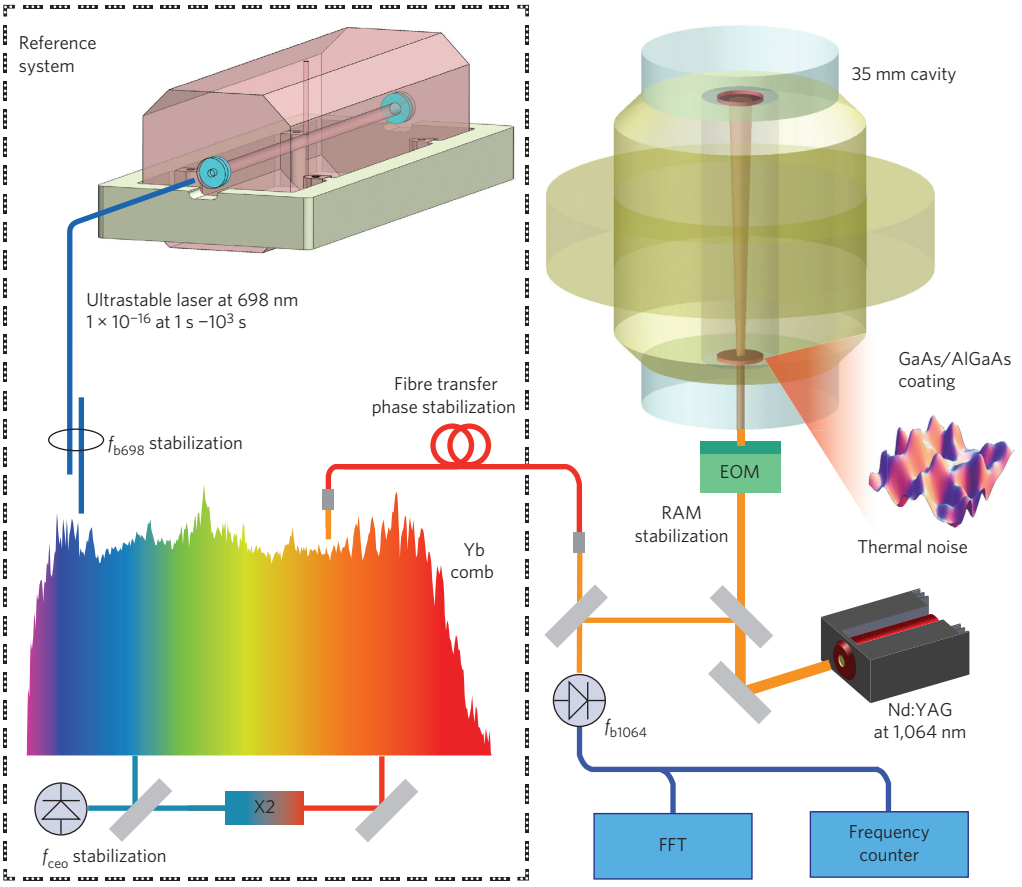

Figure 3 | Details of the thermal noise measurement system. A narrow-linewidth 698 nm laser, stabilized to a separate state-of-the-art optical cavity with a frequency stability of 1×10^{-16} from 1 to 1,000 s (ref. 11) is used as an optical reference and compared with a Nd:YAG laser at 1,064 nm stabilized to the crystalline-coating cavity. Given the large frequency difference between the lasers, a self-referenced Yb-doped fibre femtosecond frequency comb is used to transfer the stability of the 698 nm reference to 1,064 nm to facilitate a direct optical heterodyne beat comparison between the two laser/cavity systems. The residual amplitude modulation of the electro-optic modulator (EOM) used for the generation of the Pound–Drever–Hall error signal is actively stabilized to 3.5×10^{-16} at 1 s. The beat signal (f_{b1064}) is analysed with a fast Fourier transform (FFT) spectrum analyser and a frequency counter, yielding the noise properties of the cavity and crystalline coatings.

transmission stopband roughly centred at 1,064 nm (Fig. 1c). As described in the Methods, the substrate-transfer process entails removing the epitaxial layers from the native GaAs growth wafer, followed by direct bonding to the final host substrate (Fig. 2a). Using this technique, we realized high-quality compound-semiconductor-based multilayers transferred to planar and curved super-polished fused silica substrates. A photograph of a completed mirror assembly with a 1 m radius of curvature (ROC) is presented in Fig. 2b. Two of these mirrors, with crystalline coatings as the reflective elements, were optically contacted to a rigid 35-mm-long Zerodur spacer (readily available from a previous experiment[45]) so as to construct a Fabry–Pérot reference cavity (Fig. 2c). Measurement of the optical field ringdown of this resonator yielded a cavity finesse of $1.5(1) \times 10^5$ (Fig. 2d). This result is in excellent agreement with the theoretical estimate of 1.53×10^5 based on independent measurements of the transmission (4 ppm), scatter (4 ppm) and absorption (12.5 ppm) loss and is, to our knowledge, the highest finesse value ever reported for a cavity with dual single-crystal semiconductor mirrors. The exemplary optical properties observed here are attributed to the smooth interfaces and low background doping possible with an optimized MBE process. Measurement of the mode structure of the cavity revealed relatively strong birefringence, with two distinct polarization eigenmodes separated by 4.0(4) MHz, much larger than the cavity linewidth of 29 kHz. This value roughly matches a calculated maximum birefringence of 5.3 MHz (Supplementary Section S2), with the most likely origin being intrinsic strain in the epitaxial films due to differential thermal expansion of the high- and low-index layers.

Investigation of cavity stability and coating thermal noise. With the optical properties verified, the ultimate test was to probe the mechanical damping of our substrate-transferred crystalline coatings. It is a reasonable concern that the high mechanical Q values measured for suspended structures might be degraded by excess loss at the bonded interface. We therefore performed direct measurement of the thermal noise by the construction of a cavity-stabilized laser at 1,064 nm. The set-up consisted of a solid-state Nd:YAG laser precisely frequency stabilized to our crystalline-coating cavity. The short cavity length (35 mm) was chosen to make Brownian noise a dominant contribution to the overall cavity instability. To minimize noise from mechanical vibrations, the cavity was held vertically at its midplane by a ring resting on three Teflon rods[7,45] in a temperature-controlled vacuum chamber (Figs 2 and 3).

Evaluation of the cavity noise properties was realized by comparing the cavity-stabilized laser with a state-of-the-art narrow-linewidth 698 nm Sr lattice clock laser[11], which exhibits a record stability of 1×10^{-16} from 1 to 1,000 s (Fig. 3). Given the disparate operating wavelengths of the sources, we used an Yb fibre comb to

transfer the frequency stability between the reference at 698 nm and the system under test at 1,064 nm (refs 46, 47). The Yb comb output, centred at 1,050 nm with a 50 nm wavelength span, was amplified and spectrally broadened by a highly nonlinear fibre, resulting in a nearly flat and octave-spanning supercontinuum from ~700 nm to 1,400 nm. With the Yb comb phase-locked to the clock laser, the coherence of the optical reference was distributed through the entire comb spectrum. Finally, a heterodyne beat between an individual comb line and the stabilized laser at 1,064 nm, f_{b1064}, was detected and analysed, yielding the noise performance of the crystalline-coating cavity.

Figure 4a shows the fractional frequency stability σ_y (Allan deviation) of f_{b1064} measured with a frequency counter. After accounting for linear drifts in the centre frequency of the cavity-stabilized laser, the full-width at half-maximum (FWHM) linewidth of f_{b1064} was found to be 0.7 Hz (Fig. 4a, inset). With the second-order drift removed, the typical Allan deviation was $\sigma_y = 1.05(1) \times 10^{-15}$ at 1 s. Figure 4b (grey curve) presents the measured NPSD of the crystalline-coating-cavity stabilized laser. The detailed thermal noise calculation for this cavity is provided in the Methods and Supplementary Section S3. The Allan deviation and NPSD measurements are fully consistent with each other and with the predicted thermal noise floor. The calculated NPSD in the range of 1 Hz to 100 Hz is shown as the violet line in Fig. 4b, which includes the Brownian noise contributions from the spacer, substrate and coating (together shown as the dotted line in Fig. 4b), as well as the substrate thermo-elastic noise and the coating thermo-optic noise. Each of these contributions is detailed in Supplementary Table S2.

Using the known damping values for the cavity materials, we extracted a loss angle of $0(4) \times 10^{-5}$ for the substrate-transferred crystalline coatings. Because of the low loss of these coatings, the overall noise of the test cavity is dominated by contributions of the Zerodur spacer and silica substrates. Consequently, the uncertainty of the extracted result sets an upper bound for the coating loss angle, which is in general agreement with the measured room-temperature loss angle of 2.5×10^{-5} for low-frequency AlGaAs-based micromechanical resonators[38]. (An identical calculation assuming a fused-silica Q of 1×10^7 yields $\phi_{AlGaAs} = 4(4) \times 10^{-5}$, which is still in agreement with the free-standing resonator loss angle.) It is assumed that the loss angle of the coating is independent of frequency over the range investigated here. Further evidence to strengthen this assumption is provided by measurements on microfabricated AlGaAs resonators, which display a near-constant maximum Q value over more than four decades in frequency (from <200 Hz up to ~4 MHz)[38]. These results confirm that the low mechanical loss of the crystalline multilayer is maintained after the bonding process, enabling the implementation of such high-performance coatings in next-generation ultralow-thermal-noise optical interferometers. To summarize and stress the key result of the present work, Fig. 4c highlights the thermal-noise contribution of the crystalline coating itself, comprising the Brownian and thermo-optic noise of the AlGaAs multilayer. Compared with the noise of a typical amorphous SiO_2/Ta_2O_5 coating, we observe at least a factor of 10 reduction in the coating noise at 1 Hz. Owing to the additional noise contribution from thermo-optic effects, the crystalline coating is not limited solely by Brownian noise over the frequency range investigated here. However, the excess thermo-optic noise found with our current multilayer design can be reduced significantly by the addition of a half-wavelength cap (Supplementary Fig. S3).

Summary and future outlook

With the introduction of high-reflectivity end mirrors based on bonded epitaxial AlGaAs DBRs, we have demonstrated

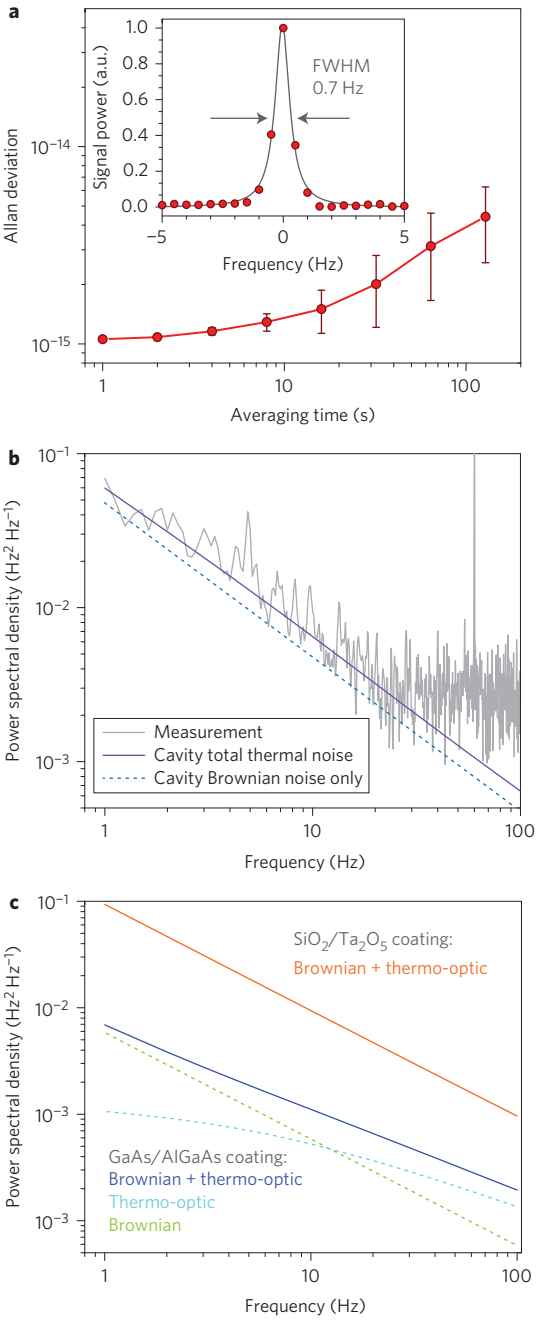

Figure 4 | Characterization of the crystalline-coating-stabilized 1,064 nm laser noise performance. a, Allan deviation: the measured f_{b1064} (red points) yields a σ_y of $1.05(1) \times 10^{-15}$ at 1 s, consistent with the theoretical estimate of 1.1×10^{-15}. Error bars denote the standard deviation for six independent measurements. Inset: measured linewidth for 10 s averaging time. The Lorentzian fit (grey line) yields a linewidth of 0.7 Hz (0.5 Hz resolution bandwidth). **b**, The stabilized laser frequency NPSD yields thermal-noise-limited performance (grey curve). Violet line: total thermal noise of the cavity based on a summation of the Brownian (coating, substrate and spacer), thermo-optic (coating) and thermo-elastic (substrate) noise contributions, assuming $\phi_{spacer} = 3 \times 10^{-4}$, $\phi_{sub} = 1 \times 10^{-6}$, $\phi_{AlGaAs} = 2.5 \times 10^{-5}$. Dashed-turquoise: cavity Brownian noise from the coating, substrate and spacer. **c**, The thermal noise for a conventional dielectric multilayer (20 periods of alternating SiO_2/Ta_2O_5 with a half-wavelength SiO_2 cap, $\phi_{dielectric} = 4 \times 10^{-4}$) is shown together with our crystalline coatings. Orange line: thermal noise of the dielectric multilayer. Blue line: thermal noise of the crystalline coating, including both the Brownian (green) and thermo-optic (cyan) noise.

unprecedentedly low Brownian noise in high-reflectivity multilayer optical coatings. The observed tenfold reduction in coating loss angle compared with state-of-the-art IBS-deposited multilayers represents a long-awaited breakthrough for the precision measurement community. Combining our crystalline coatings with optimized cavity designs will result in an immediate enhancement of the achievable frequency stability of ultranarrow-linewidth lasers, opening up the 10^{-17} stability regime at room temperature. Furthermore, the demonstrated reduction in thermal noise provides a path towards ultrastable, compact and portable laser systems and optical atomic clocks.

We anticipate immediate improvements in the optomechanical performance of these structures. As opposed to dielectric multilayers where the Q saturates or even decreases at low temperatures[48], measurements of free-standing epitaxial multilayers in a cryogenic environment reveal loss angles nearly another order of magnitude lower, down to 4.5×10^{-6} (Q of 2.2×10^5) at 10 K (ref. 38), promising substantial improvements in the thermal noise performance of next-generation cryogenic cavities. Additionally, with our microfabrication-based substrate transfer process, we foresee no fundamental barriers to realizing mirror sizes relevant for interferometric gravitational wave detectors. Finally, via bandgap engineering or simple thickness variation, as discussed in Supplementary Section S1, high-reflectivity AlGaAs DBRs can cover the wavelength range from 650 nm (ref. 49), where band-edge absorption becomes problematic, to ~3 μm (ref. 50), with the long-wavelength limit being free-carrier absorption.

Methods

Mirror fabrication. Our novel substrate-transfer coating procedure entails separating the epitaxial multilayer from the original growth wafer and directly bonding it—using no adhesives or intermediate films—to the desired mirror blank. Thus, the bonded mirror assembly initially begins as two separate components, a GaAs wafer capped with an epitaxial DBR and a super-polished fused-silica substrate with a standard backside antireflection coating. The DBR was grown using MBE on a 150-mm-diameter semi-insulating GaAs wafer and comprised alternating quarter-wave GaAs for the high-index layers and $Al_{0.92}Ga_{0.08}As$ for the low-index films. Generation of the AlGaAs mirror disc relied on standard microfabrication steps, including optical lithography to define the lateral geometry of the disc, followed by chemical etching to extrude the disc shape through the epitaxial multilayer. Chemo-mechanical substrate removal using lapping, followed by selective wet chemical etching, was used to strip the GaAs growth template. Next, the thick AlGaAs etch stop layer (Fig. 1a,b) was removed and the mirror surface was cleaned of any potential debris. Finally, the crystalline mirror disc and silica substrate were pressed into contact, resulting in a spontaneous van der Waals bond. To strengthen the interface and minimize potential frictional losses, a post-bond anneal completed the fabrication procedure.

Thermal noise theory. The single-sideband power spectral density of the thermal noise displacement (G_{total}), consisting of Brownian motion of the spacer (G_{spacer}), substrate (G_{sub}) and coating (G_{c}), as well as substrate thermo-elastic noise (G_{TE}) and coating thermo-optic noise (G_{TO}), is given by

$$\begin{aligned} G_{\mathrm{total}}(f) &= G_{\mathrm{spacer}}(f) + G_{\mathrm{sub}}(f) + G_{\mathrm{c}}(f) + G_{\mathrm{TE}}(f) + G_{\mathrm{TO}}(f) \\ &= \frac{2k_{\mathrm{B}}T}{\pi^2 f}\frac{L}{(R^2-r^2)Y_{\mathrm{spacer}}}\phi_{\mathrm{spacer}} + \frac{4k_{\mathrm{B}}T}{\pi^{3/2}f}\frac{1-\sigma_{\mathrm{sub}}^2}{w_{\mathrm{m}}Y_{\mathrm{sub}}}\phi_{\mathrm{sub}} \\ &\quad + \frac{4k_{\mathrm{B}}T}{\pi^2 f}\frac{1-\sigma_{\mathrm{sub}}^2}{w_{\mathrm{m}}Y_{\mathrm{sub}}}\frac{D}{w_{\mathrm{m}}}\frac{\phi_{\mathrm{c}}}{Y_{\mathrm{sub}}Y_{\mathrm{c}}(1-\sigma_{\mathrm{c}}^2)(1-\sigma_{\mathrm{sub}}^2)} \\ &\quad \times \left[Y_{\mathrm{c}}^2(1+\sigma_{\mathrm{sub}})^2(1-2\sigma_{\mathrm{sub}})^2 + Y_{\mathrm{sub}}^2(1+\sigma_{\mathrm{c}})^2(1-2\sigma_{\mathrm{c}})\right] \\ &\quad + G_{\mathrm{TE}}(f) + G_{\mathrm{TO}}(f) \end{aligned} \tag{1}$$

Here,

$$G_{\mathrm{TE}}(f) = \frac{8}{\sqrt{\pi}}(1+\sigma_{\mathrm{sub}})^2\alpha_{\mathrm{sub}}^2\frac{k_{\mathrm{B}}T^2 w_{\mathrm{m}}}{\kappa_{\mathrm{sub}}} \times \int_0^{+\infty}\mathrm{d}u\int_{-\infty}^{+\infty}\mathrm{d}v \sqrt{2/\pi^3}u^3 e^{-u^2/2}/\{(u^2+v^2)[(u^2+v^2)^2+\Omega_{\mathrm{TE}}^2(f)]\}$$

$$\Omega_{\mathrm{TE}}(f) = w_{\mathrm{m}}^2 C_{\mathrm{sub}}\pi f/\kappa_{\mathrm{sub}}$$

and

$$G_{\mathrm{TO}}(f) = \frac{4k_{\mathrm{B}}T^2}{\pi^{3/2}w_{\mathrm{m}}^2\sqrt{f\kappa_{\mathrm{sub}}C_{\mathrm{sub}}}}\Gamma_{\mathrm{TO}}(f)(\overline{\alpha}_{\mathrm{c}}D - \overline{\beta}_{\mathrm{c}}\lambda - \overline{\alpha}_{\mathrm{sub}}DC_{\mathrm{c}}/C_{\mathrm{sub}})^2 \quad (w_{\mathrm{m}}^2 C_{\mathrm{sub}}\pi f/\kappa_{\mathrm{sub}} \gg 1)$$

$$G_{\mathrm{TO}}(f) = \frac{4k_{\mathrm{B}}T^2}{\sqrt{\pi}w_{\mathrm{m}}\kappa_{\mathrm{sub}}}(\overline{\alpha}_{\mathrm{c}}D - \overline{\beta}_{\mathrm{c}}\lambda - \overline{\alpha}_{\mathrm{sub}}DC_{\mathrm{c}}/C_{\mathrm{sub}})^2 \quad (w_{\mathrm{m}}^2 C_{\mathrm{sub}}\pi f/\kappa_{\mathrm{sub}} \ll 1)$$

All symbols and their relevant values are defined in Supplementary Table S1. The reader is directed to the original references presented in Supplementary Section S3 for details on the underlying assumptions used in the derivation of these expressions.

The corresponding frequency noise power spectra density G_ν is

$$G_\nu(f) = G_x(f) \times \frac{\nu^2}{L^2} \tag{2}$$

Here, G_x is the thermal displacement noise corresponding to each contribution shown in equation (1), ν is optical frequency, and L is the cavity length. Equations (1) and (2) were used to calculate the thermal-noise-limited NPSD, shown as the solid violet line in Fig. 4b.

The corresponding thermal noise-limited fractional frequency stability σ_y can be determined from

$$\sigma_y^2(\tau) = \int_0^\infty \frac{G_\nu(f)}{\nu^2} \times 32\frac{(\sin(\pi f\tau/2))^4 \times \left|\sin(\pi f\tau)\right|^2}{(\pi f\tau)^4}\mathrm{d}f \tag{3}$$

The values of G_x at 1 Hz and σ_y at 1 s are summarized in Supplementary Table S2. For our current cavity configuration, Brownian noise represents the dominant contribution to the predicted total thermal noise, which gives rise to a theoretical σ_y of 1.1×10^{-15} at 1 s (compared with a measured value of $1.05(1) \times 10^{-15}$). The contribution of the coating Brownian noise is large enough (11%, as shown in Supplementary Table S2) to be isolated from competing noise sources, allowing us to determine the coating loss angle.

Received 26 February 2013; accepted 3 June 2013; published online 21 July 2013

References

1. Schiller, S. *et al.* Experimental limits for low-frequency space–time fluctuations from ultrastable optical resonators. *Phys. Rev. D* **69,** 027504 (2004).
2. Ludlow, A. D. *et al.* Sr lattice clock at 1×10^{-16} fractional uncertainty by remote optical evaluation with a Ca clock. *Science* **319,** 1805–1808 (2008).
3. Rosenband, T. *et al.* Frequency ratio of Al^+ and Hg^+ single-ion optical clocks; metrology at the 17th decimal place. *Science* **319,** 1808–1812 (2008).
4. Abbott, B. P. *et al.* LIGO: the laser interferometer gravitational wave observatory. *Rep. Prog. Phys.* **72,** 076901 (2009).
5. Saulson, P. R. Thermal noise in mechanical experiments. *Phys. Rev. D* **42,** 2437–2445 (1990).
6. Young, B. C., Cruz, F. C., Itano, W. M. & Bergquist, J. C. Visible lasers with subhertz linewidths. *Phys. Rev. Lett.* **82,** 3799–3802 (1999).
7. Ludlow, A. D. *et al.* Compact, thermal-noise-limited optical cavity for diode laser stabilization at 1×10^{-15}. *Opt. Lett.* **32,** 641–643 (2007).
8. Millo, J. *et al.* Ultrastable lasers based on vibration insensitive cavities. *Phys. Rev. A* **79,** 053829 (2009).
9. Jiang, Y. Y. *et al.* Making optical atomic clocks more stable with 10^{-16}-level laser stabilization. *Nature Photon.* **5,** 158–161 (2011).
10. Kessler, T. *et al.* A sub-40-mHz-linewidth laser based on a silicon single-crystal optical cavity. *Nature Photon.* **6,** 687–692 (2012).
11. Nicholson, T. L. *et al.* Comparison of two independent Sr optical clocks with 1×10^{-17} stability at 10^3 s. *Phys. Rev. Lett.* **109,** 230801 (2012).
12. Martin, M. J. *et al.* A quantum many-body spin system in an optical lattice clock. *Science* (in the press); preprint at http://lanl.arXiv.org/1212.6291 (2013).
13. Numata, K., Kemery, A. & Camp, J. Thermal-noise limit in the frequency stabilization of lasers with rigid cavities. *Phys. Rev. Lett.* **93,** 250602 (2004).
14. Bishof, M., Zhang, X., Martin, M. J. & Ye, J. An optical spectrum analyzer with quantum limited noise floor. Preprint at http://lanl.arXiv.org/1303.6741 (2013).
15. Callen, H. B. & Welton, T. A. Irreversibility and generalized noise. *Phys. Rev.* **83,** 34–40 (1951).
16. Landau, L. D. & Lifshitz, E. M. in *Statistical Physics* Ch. XII (Elsevier, 1996).
17. Harry, G. M. *et al.* Titania-doped tantala/silica coatings for gravitational wave detection. *Class. Quant. Grav.* **24,** 405–416 (2007).
18. Iga, K. Surface-emitting laser—its birth and generation of new optoelectronics field. *IEEE J. Sel. Top. Quant.* **6,** 1201–1215 (2000).

19. Aspelmeyer, M., Meystre, P. & Schwab, K. Quantum optomechanics. *Phys. Today* **65,** 29–35 (2012).
20. Madsen, M. *et al.* Nanoscale semiconductor 'X' on substrate 'Y'—processes, devices, and applications. *Adv. Mater.* **23,** 3115–3127 (2011).
21. Rempe, G., Thompson, R. J., Kimble, H. J. & Lalezari, R. Measurement of ultralow losses in an optical interferometer. *Opt. Lett.* **17,** 363–365 (1992).
22. Crooks, D. R. M. *et al.* Excess mechanical loss associated with dielectric mirror coatings on test masses in interferometric gravitational wave detectors. *Class. Quant. Grav.* **19,** 883–896 (2002).
23. Harry, G. M. *et al.* Thermal noise in interferometric gravitational wave detectors due to dielectric optical coatings. *Class. Quant. Grav.* **19,** 897–918 (2002).
24. Penn, S. D. *et al.* Mechanical loss in tantala/silica dielectric mirror coatings. *Class. Quant. Grav.* **20,** 2917–2928 (2003).
25. Harry, G., Bodiya, T. & DeSalvo, R. in *Gravitational Wave Detection* (eds Ottaway, D. J. & Penn, S. D.) Ch. 14, 222 (Cambridge Univ. Press, 2012).
26. Braginsky, V. B., Gorodetsky, M. L. & Vyatchanin, S. P. Thermodynamical fluctuations and photo-thermal shot noise in gravitational wave antennae. *Phys. Lett. A* **264,** 1–10 (1999).
27. Braginsky, V. B., Gorodetsky, M. L. & Vyatchanin, S. P. Thermo-refractive noise in gravitational wave antennae. *Phys. Lett. A* **271,** 303–307 (2000).
28. Evans, M. *et al.* Thermo-optic noise in coated mirrors for high-precision optical measurements. *Phys. Rev. D* **78,** 102003 (2008).
29. Gorodetsky, M. L. Thermal noises and noise compensation in high-reflection multilayer coating. *Phys. Lett. A* **372,** 6813–6822 (2008).
30. Penn, S. D. *et al.* Frequency and surface dependence of the mechanical loss in fused silica. *Phys. Lett. A* **352,** 3–6 (2006).
31. Amairi, S. *et al.* Reducing the effect of thermal noise in optical cavities. *Appl. Phys. B* http://dx.doi.org/10.1007/S00340-013-5464-8 (2013).
32. Bondarescu, M., Kogan, O. & Chen, Y. Optimal light beams and mirror shapes for future LIGO interferometers. *Phys. Rev. D* **78,** 082002 (2008).
33. Kimble, H. J., Lev, B. L. & Ye, J. Optical interferometers with reduced sensitivity to thermal noise. *Phys. Rev. Lett.* **101,** 260602 (2008).
34. Friedrich, D. *et al.* Waveguide grating mirror in a fully suspended 10 meter Fabry–Perot cavity. *Opt. Express* **19,** 14955–14963 (2011).
35. Kemiktarak, U., Metcalfe, M., Durand, M. & Lawall, J. Mechanically compliant grating reflectors for optomechanics. *Appl. Phys. Lett.* **100,** 061124 (2012).
36. Alnis, J. *et al.* Thermal-noise-limited crystalline whispering-gallery-mode resonator for laser stabilization. *Phys. Rev. A* **84,** 011804 (2011).
37. Cole, G. D., Gröblacher, S., Gugler, K., Gigan, S. & Aspelmeyer, M. Monocrystalline $Al_xGa_{1-x}As$ heterostructures for high-reflectivity high-Q micromechanical resonators in the megahertz regime. *Appl. Phys. Lett.* **92,** 261108 (2008).
38. Cole, G. D. in *Proc. SPIE 8458, Optics & Photonics, Optical Trapping and Optical Micromanipulation IX*, 8458–07 (SPIE, 2012).
39. Jewell, J. L., Scherer, A., McCall, S. L., Gossard, A. C. & English, J. H. GaAs–AlAs monolithic microresonator arrays. *Appl. Phys. Lett.* **51,** 94–96 (1987).
40. Gröblacher, S., Gigan, S., Böhm, H. R., Zeilinger, A. & Aspelmeyer, M. Radiation-pressure self-cooling of a micromirror in a cryogenic environment. *Europhys. Lett.* **81,** 54003 (2008).
41. Black, A. *et al.* Wafer fusion: materials issues and device results. *IEEE J. Sel. Top. Quant.* **3,** 943–951 (1997).
42. Bai, Y., Cole, G. D., Bulsara, M. T. & Fitzgerald, E. A. Fabrication of GaAs-on-insulator via low temperature wafer bonding and sacrificial etching of Ge by XeF_2. *J. Electrochem. Soc.* **159,** H183–H190 (2012).
43. Konagai, M., Sugimoto, M. & Takahashi, K. High efficiency GaAs thin film solar cells by peeled film technology. *J. Cryst. Growth* **45,** 277–280 (1978).
44. Yablonovitch, E., Hwang, D. M., Gmitter, T. J., Florez, L. T. & Harbison, J. P. Van der Waals bonding of GaAs epitaxial liftoff films onto arbitrary substrates. *Appl. Phys. Lett.* **56,** 2419–2421 (1990).
45. Notcutt, M. *et al.* Contribution of thermal noise to frequency stability of rigid optical cavity via hertz-linewidth lasers. *Phys. Rev. A* **73,** 031804 (2006).
46. Schibli, T. *et al.* Optical frequency comb with submillihertz linewidth and more than 10 W average power. *Nature Photon.* **2,** 355–359 (2008).
47. Benko, C. *et al.* Full phase stabilization of a Yb:fiber femtosecond frequency comb via high-bandwidth transducers. *Opt. Lett.* **37,** 2196–2198 (2012).
48. Yamamoto, K. *et al.* Measurement of the mechanical loss of a cooled reflective coating for gravitational wave detection. *Phys. Rev. D* **74,** 022002 (2006).
49. Knigge, A., Zorn, M., Wenzel, H., Weyers, M. & Trankle, C. High efficiency AlGaInP-based 650 nm vertical-cavity surface-emitting lasers. *Electron. Lett.* **37,** 1222–1223 (2001).
50. Spitzer, W. G. & Whelan, J. M. Infrared absorption and electron effective mass in n-type gallium arsenide. *Phys. Rev.* **114,** 59–63 (1959).

Acknowledgements

The authors thank M.R. Abernathy, R.X. Adhikari, A. Alexandrovski, C. Benko, T. Chalermsongsak, G.M. Harry, R. Lalezari, L-S. Ma, E. Murphy, M. Notcutt, S.D. Penn, A. Peters, P. Ullmann and R. Yanka for discussions and technical assistance. Work at the University of Vienna is supported by the Austrian Science Fund (FWF), the European Commission and the European Research Council (ERC) Starting Grant Program. The work at CMS is supported by the Austria Wirtschaftsservice GmbH (AWS) and the ERC Proof of Concept Initiative. Work at JILA is supported by the US National Institute of Standards and Technology (NIST), the DARPA QuASAR Program, and the US National Science Foundation (NSF) Physics Frontier Center at JILA. Microfabrication was carried out at the Center for Micro- and Nanostructures (ZMNS) of the Vienna University of Technology.

Author contributions

G.D.C. and M.A. designed the epitaxial multilayer, developed the substrate transfer process, and fabricated the bonded mirror assemblies. W.Z., M.J.M. and J.Y. designed and characterized the optical cavity, performed the laser frequency noise and stability measurements, and analysed the data. All authors contributed to writing the manuscript.

Additional information

Supplementary information is available in the online version of the paper. Reprints and permissions information is available online at www.nature.com/reprints. Correspondence and requests for materials should be addressed to G.D.C., J.Y. and M.A.

Competing financial interests

G.D.C. and M.A. are co-founders of a startup company (Crystalline Mirror Solutions) and co-inventors on an international patent (European Application 11010091.4) focusing on the bonded mirror technology described in the Article.